Geomechanics and Engineering, *Vol. 31, No. 1 (2022) 87-97*
https://doi.org/10.12989/gae.2022.31.1.087

Plastic deformation characteristics of disintegrated carbonaceous mudstone under dynamic loading

Xiang Qiu[1a], Yixiang Yin[1b], Huangbin Jiang*[2], Sini Fu[1b] and Jinhong Li[1b]

[1]*Department of Civil Engineering, Changsha University of Science & Technology, No. 950, Section 2, Wanjiali South Road, Tianxin District, Changsha City, Hunan Province, China*
[2]*Department of Traffic & Transportation Engineering, Changsha University of Science & Technology, No. 950, Section 2, Wanjiali South Road, Tianxin District, Changsha City, Hunan Province, China*

(*Received June 16, 2021, Revised January 28, 2022, Accepted September 18, 2022*)

Abstract. The excessive settlement and deformation of disintegrated carbonaceous mudstone (DCM) embankments under dynamic loading have long been problems for engineers and technicians. In this work, the characteristics and mechanism of the plastic deformation of DCM under different degrees of compaction, water contents and confining pressures were studied by static triaxial, dynamic triaxial and scanning electron microscopy testing. The research results show that the axial stress increases with increasing confining pressure and degree of compaction and decreases with increasing water content when DCM failure. The axial strain at failure of the DCM decreases with increasing confining pressure and degree of compaction and increases with increasing water content. Under cyclic dynamic stress, the change in the axial stress level of the DCM can be divided into four stages: the stable stage, transition stage, safety reserve stage and unstable stage, respectively. The effects of compaction, water content and confining pressure on the critical axial stress level which means shakedown of the DCM are similar. However, an increase in confining pressure reduces the effects of compaction and water content on the critical axial stress level. The main deformation of DCM is fatigue cracking. Based on the allowable critical axial stress, a method for embankment deformation control was proposed. This method can determine the degree of compaction and fill range of the embankment fill material according to the equilibrium moisture content of the DCM embankment.

Keywords: carbonaceous mudstone; critical axial stress level; cyclic dynamic stress; embankment deformation control; plastic deformation

1. Introduction

Carbonaceous mudstone is a kind of sedimentary rock composed of organic carbon, clay minerals, quartz, muscovite and feldspar. It easily disintegrates and has a low strength under the action of water (Petersen 1998, Zeng *et al*. 2021). In China, many highway and railway projects must pass through carbonaceous mudstone areas. Excavated carbonaceous mudstone is difficult to effectively use in construction due to the limitations of the existing technology, so a large amount of carbonaceous mudstone is discarded and accumulated. Under rain action, carbonaceous mudstone deposits are prone to secondary disasters such as soil erosion and mudslides. Meanwhile, an excavated carbonaceous mudstone foundation requires a large amount of high-quality fills for replacement, which undoubtedly increases the cost of engineering construction. Therefore, how to reasonably use excavated carbonaceous mudstone has become an incredibly concerning issue for engineers and technicians.

Research has shown that the particle gradation and dynamic resilience modulus of DCM can satisfy the requirements of the Chinese standard (JTG D30-2015), and DCM can be used as a fine-grained soil fill for embankments (Zhang *et al*. 2021, Chen *et al*. 2021). Therefore, in Guangxi Province and other areas where high-quality embankment fillers are quite scarce, DCM has been used as embankment fill. A series of studies on the engineering characteristics of the DCM as embankment fill were carried out (Ilori 2016, Fu *et al*. 2021, Nagrale and Patil 2017). However, embankments filled by DCM generally have undergone large settlement deformation. For example, the settlement deformation is approximately 12-18 cm at the place embankment fill thickness of approximately 6-10 m. This deformation has resulted in many cracks, dislocations and uneven subsidence of the road surface (Kim 2020, Batenipour and Alfaro 2014). The deformation of embankment fill under traffic loading can be divided into recoverable elastic deformation and unrecoverable plastic deformation (Lazorenko *et al*. 2019, Kim 2018). A critical dynamic stress will be generated in the soil under the action of cyclic loading. When the stress of the embankment fill is greater than the critical dynamic stress, plastic deformation will continue to develop until failure. When the dynamic stress of the embankment fill is less than the critical dynamic stress, the plastic deformation of the soil tends to become stable with increasing loading time (Yang *et al*. 2008, François and Karg 2010, Venkatesh *et al*. 2020, Cho

*Corresponding author, Ph.D. Student
E-mail: jianghuangbin@stu.csust.edu.cn
[a]Assistant Professor
[b]Master Degree Candidate

ISSN: 2005-307X (Print), 2092-6219 (Online)

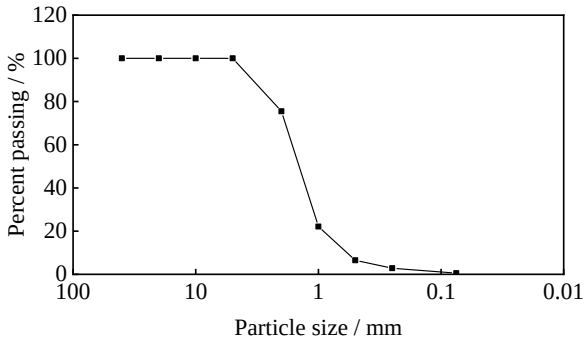

Fig. 1 Particle grading curve of the DCM

2020). The cumulative plastic deformation of the embankment fill is directly related to pavement deterioration. Therefore, determining the critical dynamic stress of embankment fill is a prerequisite for pavement structure design. At the same time, carrying out cumulative deformation testing on embankment fills is an important means to explore the factors and spatial distribution characteristics of the cumulative plastic deformation of embankment fills. This is also the basis for clarifying the influence of the accumulated plastic deformation of embankment fill on the subgrade and pavement structure.

Scholars have carried out a series of studies on the static properties of DCM embankment fill (Sadisun *et al*. 2010, He *et al*. 2014, Fu *et al*. 2020a, b). Although these research results provide an important basis to determine construction parameters when DCM is used as embankment fill, there is a lack of experimental research on the dynamic performance of DCM embankment fill. Affected by rainfall infiltration and groundwater, the critical dynamic stress and in situ stress state variation with the water content of DCM embankment fills change. In addition, the cumulative plastic deformation changes, and excessive or uneven cumulative plastic deformation destroys the subgrade and pavement (Salour and Erlingsson 2017, Ishikawa *et al*. 2014, Ren *et al*. 2012). Therefore, construction parameters such as the degree of compaction and fill range should be controlled according to the plastic deformation characteristics of the DCM embankment fill. This has important practical engineering value for the appropriate use of DCM and the control of embankment settlement and deformation.

In this paper, the plastic deformation characteristics of DCM under different compaction conditions, water contents and confining pressures were studied. The critical axial stress level envelope of the DCM was drawn. Combined with the distribution law of the axial dynamic stress with depth inside the DCM embankment, a method for embankment deformation control based on the allowable critical axial stress was proposed. This method was used to design an actual DCM embankment construction project, and good results were obtained. Thus, this method was successfully applied to the design of the construction scheme of a DCM embankment with good results.

2. Experiment details

Table 1 Physical mechanical properties of the DCM

Optimal water content (%)	Maximum dry density ($g \cdot cm^{-3}$)	Liquid limit (%)	Plastic limit (%)	Void ratio	Saturated water content (%)
18.35	1.84	47.15	21.24	0.82	30.04

Fig. 2 Static-dynamic triaxial tester

2.1 Experimental materials

The carbonaceous mudstone in the test was taken from the spoil ground of the Liuzhou-Nanning highway in Guangxi. Carbonaceous mudstone obtained on site was placed in an outdoor drying yard and naturally disintegrated after multiple drying and wet cycles. The physical and mechanical properties and particle gradation curves of the DCM are shown in Table 1 and Fig. 1, respectively.

2.2 Experimental instruments

The experiment adopted a static-dynamic three-axis experimental instrument customized for Reger, as shown in Fig. 2. The maximum static-dynamic axial load is 50 kN, the maximum axial loading rate is 10 kN/s, the maximum displacement loading rate is 31.4 mm/s, the maximum confining pressure is 1 MPa, and the maximum axial displacement is 15 cm. The control accuracy of the axial load, confining pressure and axial displacement are ±1 N, ±0.1 kPa, and ±1 μm, respectively.

The preparation method of DCM sample is as follows: the static pressure method was used for layered compaction; after compaction and static for 120 s, the layer surface was scraped; then, the next layer was compacted. Finally, a cylindrical specimen of DCM with a diameter of 100 mm and a height of 200 mm was formed.

2.3 Experimental design

According to the relevant Chinese standard (JTG D30-2015), during subgrade construction, the compaction degree of embankment packing within the range of 0-0.80 m, 0.80-1.5 m, and greater than 1.5 m from the road surface is 96%, 94%, and 93%, respectively. Considering the specification requirements and nonuniformity of compaction during embankment construction, the degrees of compaction of the DCM samples were taken as 96%, 93%, and 90%.

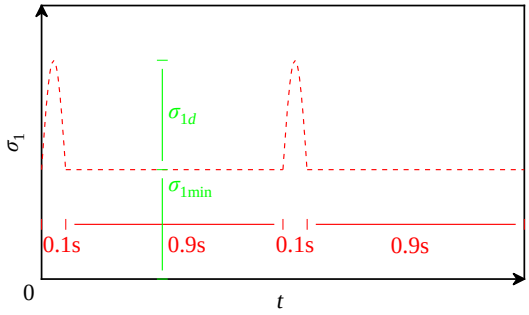

Fig. 3 Schematic diagram of the half-sine wave loading stress (σ_1 is the axial stress; t is the time; σ_{1d} is the axial dynamic stress; σ_{1min} is the minimum axial stress value)

According to the results of many investigations (Wang *et al.* 2017, Yu 2020, Feng 2021), affected by the temperature and humidity of the external environment, the water content of the embankment fill changes after filling completes and ultimately maintains a balanced value with the external environment. Considering different climate characteristics, the selected water contents of the samples were 30.14%, 24.93%, 18.35%, 12.88%, and 7.39%.

Taking a DCM embankment highway from Liuzhou to Nanning in Guangxi as an example, its relevant parameters are as follows: the maximum thickness of the embankment (h_s) was approximately 4 m and the pavement thickness (h_r) was 0.8 m, the weight of the pavement material (γ_r), weight of the embankment fill (γ_s), and lateral earth pressure coefficient (μ) were 25 kN/m^3, 20 kN/m^3, and 0.5, respectively. According to the calculation, the confining pressure on the top of the embankment was 10 kPa, and the confining pressure at 4 m below the top of the embankment was 50 kPa. Therefore, the selected confining pressures to investigate in this paper were 10 kPa, 20 kPa, 30 kPa, 40 kPa, and 50 kPa.

The expressway speed is generally 80-100 km/h, the dynamic stress loading time corresponding to this speed is approximately 0.1 s, and the dynamic stress-time history curve approximates a half-sine function (González *et al.* 2011). Therefore, a half-sine waveform loading mode with a dynamic stress action time of 0.1 s and an intermittent time of 0.9 s was selected for the test (as shown in Fig. 3), and the number of dynamic stress loadings per level was 10000 times. The specific steps of static triaxial tests are described in Qiu *et al*. (2021).

The specific steps of the triaxial tests were as follows: (i) A certain amount of distilled water was added to the DCM to make the water content of the DCM reach the optimal water content. (ii) After standing for 24 hours, the DCM was compacted in five layers by the static pressing method, and the compaction degrees were controlled to be 96%, 93%, and 90%. (iii) The compacted DCM sample was placed in a constant-temperature and -humidity chamber until the actual water content of the sample was consistent with the target water content, and the water content was controlled to be 30.14%, 24.93%, 18.35%, 12.88%, and 7.39%. (iv) The samples were transferred to the triaxial loading chamber, and the tubes of the test device were connected. Under five confining pressures (10 kPa, 2 0 kPa, 30 kPa, 40 kPa, 50 kPa), axial loads were applied (the axial loading rate was 0.01 mm/s). The failure axial stress (σ_{1f}) of the DCM under static triaxial test conditions was obtained. (v) The axial stress level (S_1') was calculated according to Eq. (1), where $\sigma_{1min}=\sigma_3$. When S_1'=75%, the dynamic triaxial test was started, the action time of dynamic stress was 0.1 s, the intermittent time was 0.9 s, and the loading times of each level of dynamic stress were 10,000 times. After the dynamic stress was applied 10,000 times, if the sample did not fail, the stress level was increased by 5%; if the sample failed, the stress level was decreased by 5%. The test was stopped when a failure stress level of the plastic stable state axial stress level and greater than 5% of the plastic stable state axial stress level appeared. At this time, the critical axial stress level of the plastic shakedown and critical axial stress level of plastic creep are defined as S_{1S}' and S_{1P}', respectively. The peak value of the critical axial plastic strain in the plastic shakedown state corresponding to S_{1S}' is defined as ε_{1pS}.

Table 2 Static and dynamic triaxial test schemes

No.	w/%	K/%	σ_3=10 kPa, 20 kPa, 30 kPa, 40 kPa, 50 kPa
1-1	18.35	96	A
			B
1-2		93	A
			B
1-3		90	A
			B
2-1	30.14	96	A
			B
2-2	24.93		A
			B
2-3	18.35		A
			B
2-4	12.88		A
			B
2-5	7.39		A
			B

$$S_1' = \sigma_{1max} / \sigma_{1f} \tag{1}$$

where S_1' is the axial stress level and $\sigma_{1max}=\sigma_{1d}+\sigma_{1min}$ is the peak axial stress of the dynamic triaxial test.

The axial plastic strain is expressed as ε_{1p} and calculated using Eq. (2).

$$\varepsilon_{1p} = \frac{|l' - l|}{l} \tag{2}$$

where ε_{1p} is the plastic axial strain, l' is the height of the sample when $\sigma_{1d}=0$, and l is the height of the sample before the test.

2.4 Experimental programme

The main purpose of this work was to study the effects of the degree of compaction (K), confining pressure (σ_3), and water content (w) on the static and dynamic

Table 3 Results of static and dynamic triaxial tests

No.	w/%	K/%	σ_{1f}, ε_{1f}	σ_3=10 kPa	σ_3=10 kPa	σ_3=10 kPa	σ_3=10 kPa	σ_3=10 kPa
1-1	18.35	96	σ_{1f}/kPa	68.97	93.33	118.94	144.43	167.90
			ε_{1f}/%	7.04	4.34	2.86	2.20	2.08
1-2		93	σ_{1f}/kPa	60.36	83.59	106.86	129.98	153.8
			ε_{1f}/%	8.27	5.42	3.84	3.08	2.60
1-3		90	σ_{1f}/kPa	46.64	66.82	87.52	108.31	128.2
			ε_{1f}/%	11.81	7.17	5.00	4.37	3.42
2-1	30.14	96	σ_{1f}/kPa	41.46	68.52	90.34	115.11	139.5
			ε_{1f}/%	11.24	6.65	4.64	3.62	3.34
2-2	24.93		σ_{1f}/kPa	61.76	86.32	111.07	137.17	160.61
			ε_{1f}/%	8.76	5.18	3.82	2.92	2.52
2-3	18.35		σ_{1f}/kPa	68.97	93.33	118.94	144.43	167.90
			ε_{1f}/%	7.04	4.34	2.86	2.20	2.08
2-4	12.88		σ_{1f}/kPa	86.88	111.59	136.70	160.59	186.96
			ε_{1f}/%	6.10	3.97	2.62	1.98	1.89
2-5	7.39		σ_{1f}/kPa	98.9	125.31	148.79	172.63	199.7
			ε_{1f}/%	11.24	6.65	4.64	3.62	3.34

performance of the DCM (axial stress of failure (σ_{1f}), axial strain of failure (ε_{1f}), critical axial stress level of the plastic shakedown (S_{1S}') and critical axial stress level of the plastic creep failure (S_{1P}') of the DCM under static stress). Electron scanning microscopy of DCM was carried out before and after dynamic stress loading to analyse the plastic deformation mechanism of DCM under the action of dynamic stress. The specific experimental programme is shown in Table 2. In this table, A represents the static triaxial test, B represents the dynamic triaxial test, and $\sigma_{1min}=\sigma_3$.

The initial axial stress level of the dynamic triaxial test was 75%. To obtain S_{1S}' under the action of the dynamic stress and the stress level where failure occurs when S_{1P}' is greater than 5%, the axial stress level of the dynamic triaxial was adjusted according to the failure state of the sample (when failure occurs, the stress level is increased by 5%; when the sample is damaged, the stress level is reduced by 5%). In addition, the peak axial plastic strain corresponding to S_{1S}' was defined as the critical axial plastic strain in the plastic shakedown state (ε_{1pS}).

3. Results and discussion

3.1 σ_{1f} and ε_{1f} of the DCM

The static and dynamic triaxial test results of the DCM are shown in Table 3. σ_{1f} of the DCM is positively correlated with the confining pressure and degree of compaction but negatively correlated with the water content. ε_{1f} of the DCM is negatively correlated with the confining pressure and degree of compaction and positively correlated with the water content. This occurs mainly because the increase in confining pressure, degree of compaction and lateral restraint of the rock and soil results in denser carbonaceous mudstone particles. Thus, the corresponding σ_{1f} required for the specimen to undergo shear failure is larger, and the corresponding ε_{1f} is smaller. In addition, when the sample contains more water, the matrix suction and bite force between the carbonaceous mudstone particles are lower, which leads to a lower σ_{1f} and higher ε_{1f} when shear failure occurs (Gao *et al.* 2018).

(a) before the test (b) after the test

Fig. 4 Comparative images of a representative sample before and after the test

3.2 Axial plastic strain characteristics of the DCM

When K=96%, σ_3=30 kPa, and S_1'=95%, the comparative image of a representative sample before and after the test is shown in Fig. 4. The DCM sample did not undergo shear failure before the axial strain reached 20%, but a lateral deformation bulge occurred near one-third of the sample height from the bottom of the sample.

The relationships between the axial plastic strain of the DCM and the number of dynamic stress loadings are shown in Fig. 5. The ε_{1p}-n curve exhibits the following trends:

When σ_3=30 kPa and S_1'=90%, the change in axial plastic strain of the DCM can be divided into the plastic deformation stage ($n\leq1000$), plastic shakedown stage ($1000<n\leq3000$) and plastic accumulation failure stage. In the plastic deformation stage, the pores between the rock and soil particles are continuously compacted, and the axial plastic strain of the sample increases first and subsequently stabilizes. In the plastic shakedown stage, the rock and soil particles are relatively dense, and the sample produces only

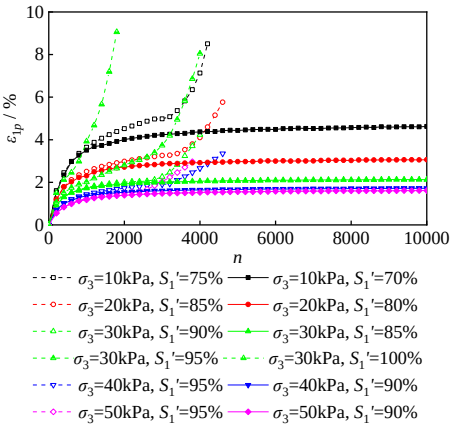

(a) No. 1-1

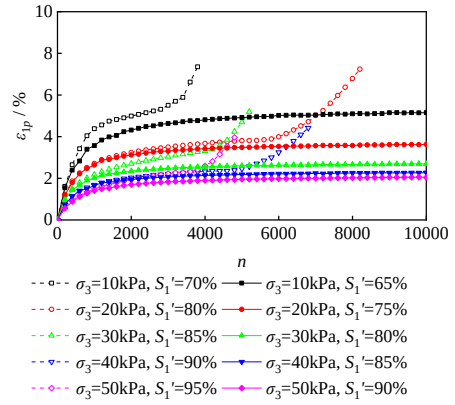

(b) No. 1-2

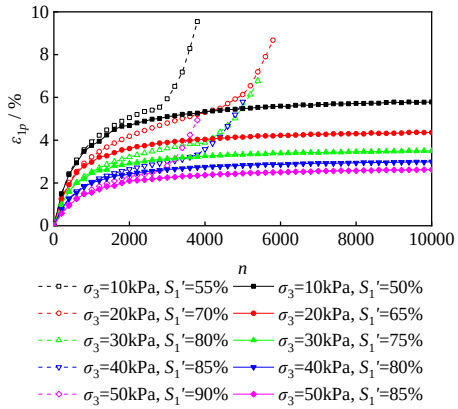

(c) No. 1-3

Fig. 5 ε_{1p}-n curve of the DCM

a small axial plastic strain or axial elastic strain. In the plastic accumulation failure stage, plastic shear failure occurs between the rock and soil particles, the axial plastic strain of the specimen rapidly increases, and the slope of the curve also increases. Therefore, the ε_{1p}-n curve reflects a state of plastic creep failure.

When σ_3=30 kPa and S_1'=85%, the change in axial plastic strain of DCM can be divided into the plastic deformation stage (n≤1000) and plastic shakedown stage (n>1000). In the plastic deformation stage, the axial plastic strain of the specimen rapidly accumulates with more loading cycles, and the strain increment gradually decreases; in the plastic shakedown failure stage, the axial

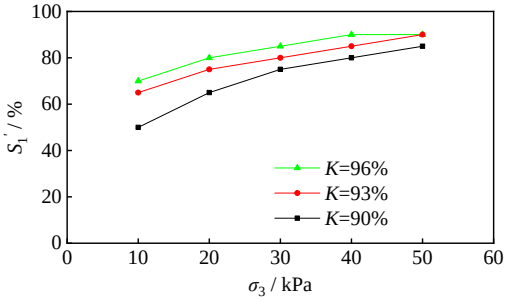

Fig. 6 S_{1S}' of the DCM under different degrees of compaction and confining pressures

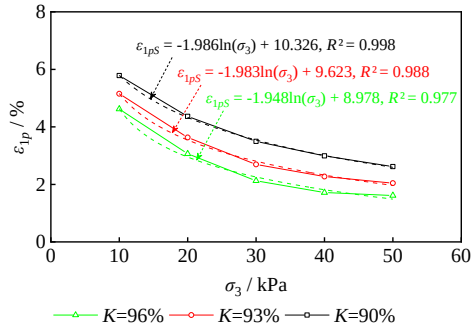

Fig. 7 ε_{1pS} of the DCM under different degrees of compaction and confining pressures

plastic strain increment continues to increase. Therefore, the ε_{1p}-n curve reflects a state of plastic shakedown.

When σ_3=30 kPa and S_1'=95%, the change in axial plastic strain of the DCM can be divided into the plastic deformation stage (n≤1000) and plastic accumulation failure stage (n>1000). In the plastic deformation stage, the axial plastic strain of the specimen rapidly accumulates with more loading cycles, and the strain increment gradually decreases; in the plastic accumulation failure stage, the axial plastic strain increment continues to increase. Therefore, the ε_{1p}-n curve reflects a state of plastic cumulative failure.

In summary, the ε_{1p}-n curve of the DCM can describe three states under the action of different stress levels and loading times: plastic creep failure, plastic shakedown, and plastic cumulative failure. The DCM has a critical axial stress level that corresponds to a stable plastic state under the action of dynamic stress. When the axial stress level of the DCM is less than the critical axial stress level in the plastic shakedown state, the permanent axial deformation first rapidly accumulates and subsequently stabilizes. At this time, the DCM is in a state of plastic shakedown. When the axial stress level of the DCM is greater than the critical axial stress level in the stable plastic state, the permanent axial deformation continues to accumulate until overall shear failure occurs, at which time the DCM is in a state of plastic cumulative failure. The continuous increase in permanent axial deformation of the embankment fill induces pavement cracking and other issues. Therefore, to ensure the quality of the project, the maximum S_{1S}' is generally considered the critical axial stress level of the plastic shakedown state.

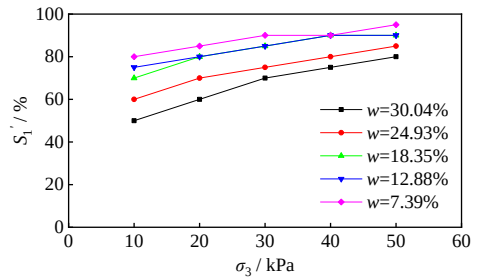

Fig. 8 S_{1S}' of the DCM under different water contents and confining pressures

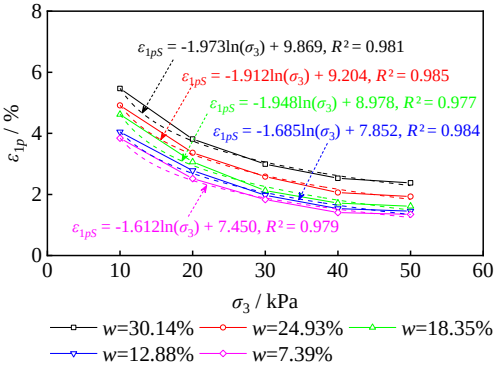

Fig. 9 ε_{1pS} of the DCM under different water contents and confining pressures

3.3 Influence of the degree of compaction and confining pressure on S_{1S}' and ε_{1pS}

S_{1S}' and ε_{1pS} of the tested DCM under different compaction degrees and confining pressures are shown in Fig. 6 and Fig. 7, respectively. Notably, S_{1S}' of the DCM is positively correlated with the degree of compaction and confining pressure under identical water content. When the degree of compaction is large, the extent of the reduction in S_{1S}' decreases with decreasing confining pressure (when the confining pressure is reduced from 50 kPa to 10 kPa, the axial stress levels of the DCM with degrees of compaction of 96%, 93%, and 90% decrease by 20%, 25%, and 30%, respectively). When the confining pressure is large, the extent of the reduction in S_{1S}' decreases with decreasing degree of compaction (when the degree of compaction is reduced from 96% to 90%, the axial stress levels of the DCM with confining pressures of 50 kPa, 40 kPa, 30 kPa, 20 kPa, and 10 kPa decrease by 5%, 10%, 10%, 15%, and 20%, respectively). The reason for this phenomenon is that DCM with a larger degree of compaction has greater compactness, which also makes the DCM have a higher lateral constraint. Therefore, a denser sample can better resist deformation.

ε_{1pS} of the DCM is negatively correlated with the degree of compaction and confining pressure under identical water contents. When the confining pressure is small, ε_{1pS} of the DCM nonlinearly increases with decreasing confining pressure (the axial strain increment continues to increase). The relationship between ε_{1pS} and the confining pressure of the DCM with different degrees of compaction can be fitted by the logarithmic function ($\varepsilon_{1pS} = a\ln(\sigma_3) + b$, a<0), as shown in Fig. 5, and the fitting effect is strong (R^2>0.95). Parameter a is positively correlated with the degree of compaction, and parameter b is negatively correlated with the degree of compaction. Thus, it is of great significance to control the plastic deformation of the embankment from the perspective of improving the degree of compaction of the DCM.

3.4 Influences of the water content and confining pressure on S_{1S}' and ε_{1pS}

S_{1S}' and ε_{1pS} of the DCM under different water contents and different confining pressure conditions are shown in Fig. 8 and Fig. 9, respectively. Notably, S_{1S}' of the DCM is negatively correlated with the water content and positively correlated with the confining pressure under identical degrees of compaction. When the water content is large, the extent of the reduction in S_{1S}' decreases with increasing confining pressure (when the confining pressure is reduced from 50 kPa to 10 kPa, the axial stress levels of the DCM with water contents of 30.04%, 24.93%, 18.35%, 12.88% and 7.39% decrease by 30%, 25%, 20%, 15% and 15%, respectively). When the confining pressure is high, the extent of the reduction in S_{1S}' decreases with decreasing degree of compaction (when the water content is increased from 7.39% to 30.04%, the axial stress levels of the DCM with confining pressures of 50 kPa, 40 kPa, 30 kPa, 20 kPa, and 10 kPa decrease by 15%, 15%, 20%, 25%, and 30%, respectively). The reason for this phenomenon is that a greater degree of compaction corresponds to a more compact DCM, and a greater confining pressure corresponds to a greater lateral constraint of the DCM. Taking the axial stress level of the DCM with a water content of 18.35% as a benchmark, with the increase in water content, the increase in axial stress level is greater than the decrease in water content.

ε_{1pS} of the DCM is positively correlated with the water content and negatively correlated with the confining pressure under identical degrees of compaction. The logarithmic function ($\varepsilon_{1pS} = a\ln(\sigma_3) + b$, a<0) can effectively fit the relationship between ε_{1pS} and the confining pressure of DCM with different water contents. Parameter a is negatively correlated with the water content, and parameter b is positively correlated with the water content.

3.5 Analysis of the microstructure of DCM

To reveal the structural failure mechanism of DCM, the fresh fracture surface of the DCM was vacuum-coated with gold for observations. SEM imaging was performed in a HELIOS Nano Lab 600i field-emission SEM system (EDAX Ltd., JSM, USA) at 20 kV.

Fig. 10 shows scanning electron microscopy images of DCM before and after dynamic triaxial testing. The DCM before the dynamic triaxial testing is structurally complete and has no obvious cracks, and the DCM thin section surface is smooth and flat (as shown in Fig. 10(a)). After the dynamic triaxial testing, some fissures and shedding holes

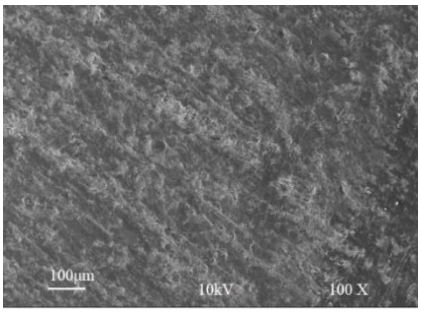

(a) before the dynamic triaxial testing

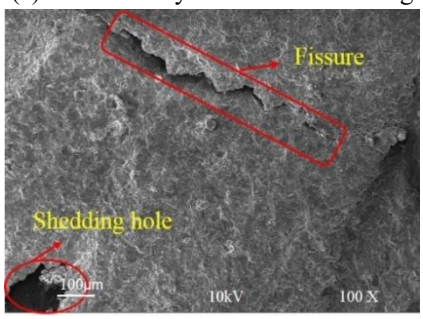

(b) after the dynamic triaxial testing

Fig. 10 Scanning electron microscopy images of DCM

were observed in the DCM, and the roughness of the thin section surface of the DCM significantly increased (as shown in Fig. 10(b)). During the action of cyclic dynamic stress, carbonaceous mudstone particles separated and fell from the surface of the DCM sample, and fatigue cracks formed at the stress concentrations. Eventually, the skeleton structure of DCM was destroyed, and its strength was reduced. Thus, the axial stress of the DCM under dynamic stress was smaller than the axial stress of the DCM under static stress (when the stress level was below 100%).

4. Project case analysis

Field tests were conducted on the carbonaceous mudstone embankment of the highway from Liuzhou city to Nanning city in Guangxi Province, China. The distribution of the maximum axial dynamic stress (ε_{1hd}) at different depths below the road surface was obtained by field tests under the condition of the vehicle driving speed was 100 km/h and the axle load of the single-axle two-wheel group was 100 kN. As shown in Fig. 11, the measured maximum axial dynamic stress at the top surface of the embankment (h=0 m) is 26.03 kPa, and the measured maximum axial dynamic stress at the bottom surface of the embankment (h=4 m) is 2.87 kPa. The maximum axial dynamic stress inside the embankment rapidly decreases with increasing depth, and the rate of decrease in maximum axial dynamic stress inside the embankment gradually decreases with increasing depth. In addition, the relationship between axial dynamic stress and depth of the embankment was fitted with an exponential function ($\sigma_{1hd} = a'e^{(b'h)}$).

According to the theory of shakedown, if the stress level of the embankment fill is less than the critical stress level of the plastic shakedown, the embankment gradually becomes

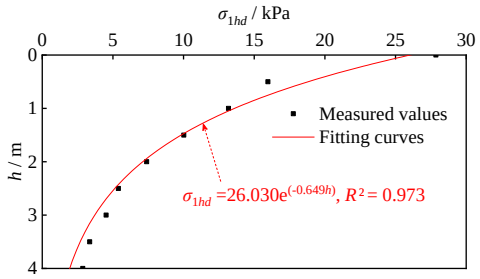

Fig. 11 Relationship between axial dynamic stress and depth of the embankment

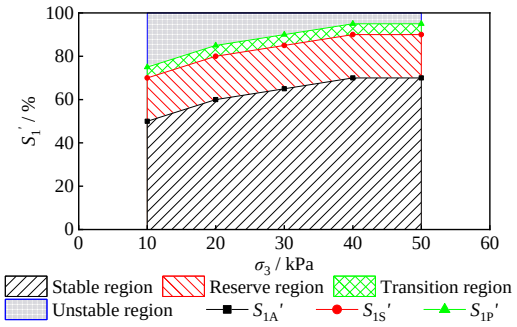

Fig. 12 Critical axial stress level envelope of the DCM (w=30.04%, K=96%)

stable after a certain amount of plastic deformation. To ensure the safety, reliability and stability of embankment construction, the unevenness of the compaction of embankment fill material and the influence of uncertain factors such as heavy-duty vehicle traffic must be comprehensively considered. According to the requirements of the safety reserve of an expressway embankment (Chinese standard (JTG D30-2015)), a stress level below 20% of the critical stress level in the plastic shakedown state is considered the critical axial stress level of the allowable material (S_{1A}'). Fig. 12 shows the critical axial stress level envelope of the DCM. The region above S_{1P}' is the unstable region. The region between S_{1P}' and S_{1S}' is the transition region. The region between S_{1S}' and S_{1A}' is the safety reserve region. The region below S_{1A}' is the stable region.

The allowable critical axial stress (σ_{1A}) of an embankment packing at different depths is the product of the allowable critical axial stress level (S_{1A}') and failure axial stress (σ_{1f}). According to the parameters of the subgrade and pavement, the axial stress at the top surface of the embankment ($\sigma_{1h=0}=\gamma_r h_r$) is 20 kPa, and the confining pressure ($\sigma_{3h=0}=\gamma_r h_r \mu$) is 10 kPa. Therefore, the expressions of the axial stress (σ_{1h}), confining pressure (σ_{3h}), and peak axial stress of embankment packing at different depths (σ_{1hmax}) are given in Eqs. (3)-(5).

$$\sigma_{1h} = \sigma_{1h=0} + \gamma_s h \tag{3}$$

$$\sigma_{3h} = \sigma_{3h=0} + \gamma_s h\mu \tag{4}$$

$$\sigma_{1h\,max} = \sigma_{1h} + \sigma_{1hd} \tag{5}$$

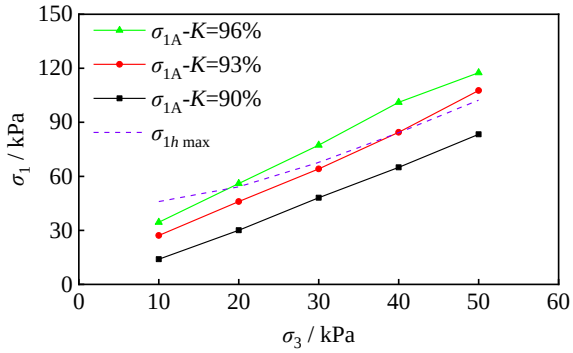

Fig. 13 Curves of σ_{1A} and σ_{1hmax} of the DCM with different degrees of compaction

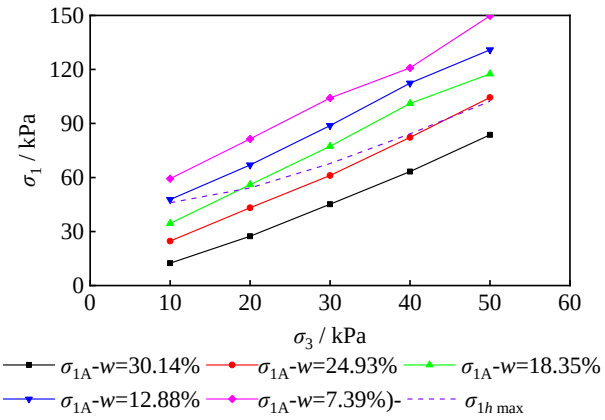

Fig. 14 Curves of σ_{1A} and σ_{1hmax} of the DCM with different water contents

Each time the depth of the embankment increases by 1 m, σ_{1A}, σ_{1h}, σ_{3h} and σ_{1hmax} are calculated by the above method. The curves of the allowable critical axial stress and the axial stress peak value versus confining pressure of the DCM with different degrees of compaction and water contents are shown in Fig. 13 and Fig. 14, respectively. When the equilibrium water content of the embankment fill is equal to the optimal water content, the peak axial stress of the fill with different degrees of compaction within 0.9 m from the top surface of the embankment is greater than the allowable critical axial stress. In this range, it is necessary to use high-quality embankment fill for replacement. The control standard for the degree of compaction of the fill within the range of 0.9-3 m below the top of the embankment should be greater than or equal to 96%, and the control standard for the degree of compaction of the fill within the range of 3 m below the top of the embankment should be greater than or equal to 93%. When the degree of compaction of the embankment fill is 96% and the equilibrium water content is less than or equal to 12.88%, DCM can be used to fill the entire embankment. When the equilibrium water content is 24.93%, DCM can be used as the embankment fill within 3.5 m from the top surface of the embankment. When the equilibrium water content is equal to the saturated water content, DCM cannot be used as the embankment fill.

5. Discussion

Based on the analysis of the static and dynamic triaxial test results of the DCM, an embankment deformation control method based on allowable critical axial stress was proposed. This method can determine the degree of compaction and fill range of the embankment fill material according to the equilibrium water content of the DCM embankment and has important guiding significance for the appropriate utilization of DCM and other undesirable fills. However, in this study, the confining pressures of different embankment depths were estimated using empirical estimates (assuming that the coefficient of lateral earth pressure of the embankment fill inside the embankment is 0.5), and the axial plastic strain under each axial stress level was not actually tested. Therefore, it was impossible to accurately predict the settlement deformation of the embankment under vehicle loading. To further improve the accuracy of the new method of embankment deformation control, in follow-up work, confining pressure tests at different embankment depths and dynamic triaxial tests at different axial stress levels must be carried out.

6. Conclusions

To solve the problem of the large settlement and deformation of DCM embankments under dynamic loading, a method for testing the plastic deformation characteristics of DCM under dynamic loading was proposed. Using this method, the critical axial stress level of plastic shakedown and critical axial stress level of plastic creep of DCM under different compaction levels, water contents and confining pressures were determined.

- The axial stress of the DCM is positively correlated with the confining pressure and degree of compaction and negatively correlated with the water content. The failure axial strain of the DCM is negatively correlated with the confining pressure and degree of compaction and positively correlated with the water content.
- The characteristics of the axial plastic strain of the DCM under cyclic dynamic stress can be divided into three states: the plastic creep failure state, plastic shakedown state, and plastic cumulative failure state. The axial stress level can be divided into four stages: the stable stage, transition stage, safety reserve stage and unstable stage.
- Under the same water content, the critical axial stress level of the DCM in the plastic shakedown state is positively correlated with the confining pressure and degree of compaction; the critical axial strain in the plastic shakedown state is negatively correlated with the confining pressure and degree of compaction. Under the same degree of compaction, the critical stress level of the DCM is negatively correlated with the water content and positively correlated with the confining pressure; the critical axial strain during stable plastic shakedown is positively correlated with the water content and negatively correlated with the confining pressure. Under the action of cyclic dynamic stress, carbonaceous

mudstone particles separated and fell from the surface of the DCM sample, and fatigue cracks formed at the locations of stress concentrations. Eventually, the skeleton structure of DCM was destroyed, and its strength was also reduced.

• To ensure the long-term safety and stability of the embankment, the axial stress level of the embankment should be designed to remain in the stable stage; that is, the allowable critical axial stress envelope should be taken as the upper limit for embankment axial stress control.

Acknowledgements

The research described in this paper was financially supported by the National Natural Science Foundation of China (Nos. 52278439, 51908073, 51838001 and 52078066), and the Natural Science Foundation Project of Hunan Provincial Department of Education (21B0317).

References

Batenipour, H., Alfaro, M., Kurz, D. and Graham, J. (2014), "Deformations and ground temperatures at a road embankment in northern Canada", *Can. Geotech. J.*, **51**(3), 260-271. http://dx.doi.org/10.12989/gae.2020.20.2.103.

Chen, H.H., Li, L, Li, J.P. and Sun, D.A. (2021), "A generic analytical elastic solution for excavation responses of an arbitrarily-shaped deep opening under biaxial in-situ stresses", *Int. J. Geomech.*, **22**(4), 04022023., https://doi.10.1061/(ASCE)GM.1943-5622.0002335.

Cho, H.I., Kim, H.S., Sun, C.G. and Kim, D.S. (2020), "Settlement prediction for footings based on stress history from V S measurements", *Geomech. Eng.*, **20**(5), 371-384. https://doi.org/10.12989/gae.2020.20.5.371.

Feng, R., Wang, L., Wei, K. and Zhao, J. (2021), "Consolidation settlement of soil foundations containing organic matters subjected to embankment load", *Geomech. Eng.*, **24**(1), 43-55. https://doi.org/10.12989/gae.2021.24.1.043.

François, S., Karg, C., Haegeman, W. and Degrande, G. (2010), "A numerical model for foundation settlements due to deformation accumulation in granular soils under repeated small amplitude dynamic loading", *Int. J. Numer. Anal. Meth. Geomech.*, **34**(3), 273-296. https://doi.org/10.1002/nag.807.

Fu, H. and Chen, C. (2020), "Effect of nanotalc on the shear strength of disintegrated carbonaceous mudstone", *J. Nanosci. Nanotechnol.*, **20**(8), 5049-5054. https://doi.org/10.1166/jnn.2020.18490.

Fu, H., Chen, C., Zha, H., Yuan, D., Gao, Q.F., Zeng, L. and Jia, C. (2021), "Hydrophobic polymeric additives toward a long-term robust carbonaceous mudstone slope", *Polym.*, **13**(5), 802. https://doi.org/10.3390/polym13050802.

Gao, Q.F., Dong, H., Huang, R. and Li, Z.F. (2019), "Structural characteristics and hydraulic conductivity of an eluvial-colluvial gravelly soil", *Bull. Eng. Geol Environ.*, **78**(7), 5011-5028. https://doi.org/10.1007/s10064-018-01455-1.

González, A., Cantero, D. and OBrien, E.J. (2011), "Dynamic increment for shear force due to heavy vehicles crossing a highway bridge", *Comput. Struct.*, **89**(23-24), 2261-2272. https://doi.org/10.1016/j.compstruc.2011.08.009.

He, Z.M., Xiang, D. and Liu, Y.X. (2020), "Triaxial creep test and particle flow simulation of coarse-grained soil embankment filler", *Front. Earth Sci.*, **8**, 62. https://doi.org/10.3389/feart.2020.000629.

Ilori, A.O. (2016), "Occurrence of shale soils along the Calabar-Itu highway, Southeastern Nigeria and their implication for the subgrade construction", *SpringerPlus*, **5**(1), 1-13. https://doi.org/10.1186/s40064-016-1822-4.

Ishikawa, T., Miura, S. and Sekine, E. (2014), "Simple plastic deformation analysis of ballasted track under repeated moving-wheel loads by cumulative damage model", *Transp. Geotech.*, **1**(4), 157-170. https://doi.org/10.1016/j.trgeo.2014.06.006.

Kim, N.Y., Park, D.H., Jung, H.S. and Kim, M.I. (2020), "Deformation characteristics of tunnel bottom after construction under geological conditions of long-term deformation", *Geomech. Eng.*, **21**(2), 171-178. https://doi.org/10.12989/gae.2020.21.2.171.

Kim, Y., Dang, M.Q., Do, T.M. and Lee, J.K. (2018), "Soil stabilization by ground bottom ash and red mud", *Geomech. Eng.*, **16**(1), 105-112. https://doi.org/10.12989/gae.2018.16.1.105.

Lazorenko, G., Kasprzhitskii, A., Khakiev, Z. and Yavna, V. (2019), "Dynamic behavior and stability of soil foundation in heavy haul railway tracks: A review", *Constr. Build. Mater.*, **205**, 111-136. https://doi.org/10.1016/j.conbuildmat.2019.01.184.

Nagrale, P.P. and Patil, A.P. (2017), "Improvement in engineering properties of subgrade soil due to stabilization and its effect on pavement response", *Geomech. Eng.*, **12**(2), 257-267. http://doi.org/10.12989/gae.2017.12.2.257.

Petersen, H.I. (1998), "Morphology, formation and palaeo-environmental implications of naturally formed char particles in coals and carbonaceous mudstones", *Fuel*, **77**(11), 1177-1183. https://doi.org/10.1016/S0016-2361(98)00021-0.

Qiu, X., Li, J., Jiang, H., Fu, H. and Yang, S. (2021), "A nonlinear constitutive model for disintegrated carbonaceous mudstone based on logarithmic functions", *Adv. Civil Eng.*, **2021**, Article ID 6690169. https://doi.org/10.1155/2021/6690169.

Ren, X.W., Tang, Y.Q., Li, J. and Yang, Q. (2012), "A prediction method using grey model for cumulative plastic deformation under cyclic loads", *Nat. Hazard.*, **64**(1), 441-457. https://doi.org/10.1007/s11069-012-0248-8.

Sadisun, I.A., Bandono, B., Shimada, H., Ichinose, M. and Matsui, K. (2010), "Physical disintegration characterization of mudrocks subjected to slaking exposure and immersion tests", *Indones. J. Geosci.*, **5**(4), 219-225. https://:doi.org/10.17014/ijog.v5i4.105.

Salour, F. and Erlingsson, S. (2017), "Permanent deformation characteristics of silty sand subgrades from multistage RLT tests", *Int. J. Pave. Eng.*, **18**(3), 236-246. https://doi.org/10.1080/10298436.2015.1065991.

Venkatesh, N., Heeralal, M. and Pillai, R.J. (2020), "Resilient and permanent deformation behaviour of clayey subgrade soil subjected to repeated load triaxial tests", *Eur. J. Environ. Civil Eng.*, **24**(9), 1414-1429. https://doi.org/10.1080/19648189.2018.1472041.

Wang, J.D., Gu, T.F. and Xu, Y.J. (2017), "Field tests of expansive soil embankment slope deformation under the effect of the rainfall evaporation cycle", *Appl. Ecol. Environ. Res.*, **15**(3), 343-357. http://doi.org/10.15666/aeer/1503_343357.

Yang, S.R., Huang, W.H. and Liao, C.C. (2008), "Correlation between resilient modulus and plastic deformation for cohesive subgrade soil under repeated loading", *Transp. Res. Record*, **2053**(1), 72-79. https://doi.org/10.3141/2053-09.

Yu, Y., Wang, Z. and Sun, H. (2020), "Optimal design of stone columns reinforced soft clay foundation considering design robustness", *Geomech. Eng.*, **22**(4), 305-318. https://doi.org/10.12989/gae.2020.22.4.305.

Zeng, L., Yu, H.C., Liu, J., Gao, Q.F. and Bian, H.B. (2021), "Mechanical behaviour of disintegrated carbonaceous mudstone under stress and cyclic drying/wetting", *Constr. Build. Mater.*,

282, 122656. https://doi.org/10.1016/j.conbuildmat.2021.122656.
Zhang, J., Peng, J., Zeng, L., Li, J. and Li, F. (2019), "Rapid estimation of resilient modulus of subgrade soils using performance-related soil properties", *Int. J. Pave. Eng.*, **22**(6), 732-739. https://doi.org/10.1080/10298436.2019.1643022.

CC

Notations

K	degree of compaction
w	water content
n	number of dynamic stress loadings
h	depth below the road surface
h_r	thickness of pavement
h_s	thickness of embankment
γ_r	gravity of pavement materials
γ_s	gravity of embankment fill
σ_3	confining pressure
σ_1	axial stress
σ_{1min}	minimum axial stress
σ_{1max}	peak axial stress
σ_{1h}	axial dynamic stress at different depth below the road surface
σ_{3h}	confining pressure at different depths below the road surface
σ_{1hmax}	peak axial stress of embankment packing at different depths
σ_{1f}	failure axial stress
σ_{1d}	axial dynamic stress
ε_{1hd}	maximum axial dynamic stress at different depths below the road surface
ε_{1f}	axial strain of failure
S_{1S}'	critical axial stress level of the plastic shakedown
S_{1P}'	critical axial stress level of the plastic creep failure
S_{1A}'	critical axial stress level of the allowable material
S_1'	axial stress level
ε_{1pS}	critical axial plastic strain in the plastic shakedown state
ε_{1p}	peak axial plastic strain
a	fitting parameter
b	fitting parameter